DOI: 10.1002/((please add manuscript number))
Article type: Communication

Title : Charge transport in two-dimensional DNA tunnel junction diodes

*Minho Yoon, Sung-Wook Min, Sreekantha Reddy Dugasani, Yong Uk Lee, Min Suk Oh, Thomas D. Anthopoulos, Sung Ha Park and Seongil Im**

Dr. Minho Yoon, Mr. Sung-Wook Min, Prof. Seongil Im
Department of Physics, Yonsei University, Seoul 120-749, Korea.

Dr. Sreekantha Reddy Dugasani , Prof. Sung Ha Park
Department of Physics, Sungkyunkwan University, Suwon 440-746, Korea.

Dr. Yong Uk Lee
Material Research Centre, Samsung Advanced Institute of Technology, Suwon, 16678, Korea.

Dr. Min Suk Oh
Display Materials & Components Research Center, Korea Electronics Technology Institute, Seongnam 463-816, Korea.

Prof. Thomas D. Anthopoulos
Materials Science and Engineering Division of Physical Sciences and Engineering, King Abdullah University of Science and Technology, Thuwal 23955-6900, Saudi Arabia.

E-mail: semicon@yonsei.ac.kr

Keywords: nanosheet, two-dimensional DNA crystal, semitransparent conducting oxide, tunnel junction diode, charge-transport mechanisms

Abstract

Recently, DNA has been studied for electronics due to its intrinsic benefits such as its natural plenitude, bio-degradability, bio-functionality and low-cost. However, its applications only limit to passive components because of inherent insulating properties. In this report, the metal-insulator-metal tunnel diode with Au/DNA/NiO_x junctions is presented. Through the self-aligning process of DNA molecules, a two dimensional DNA nanosheet is synthesized and used as a tunneling barrier, and semitransparent conducting oxide, NiO_x is applied as a top electrode for resolving metal penetration issues. These molecular devices successfully operate as a non-resonant tunneling diode and temperature-variable current-voltage analysis

proves that Fowler–Nordheim tunneling is a dominant conduction mechanism in the junctions. The DNA-based tunneling devices appear to be a promising prototype approach to nanoelectronics using biomolecules.

Deoxyribonucleic acid (DNA) is a macromolecule that stores the genetic information of all known living organisms. DNA consists of long strands of alternating sugar and phosphate groups along with the four types of nitrogenous bases: adenine (A), thymine (T), guanine (G) and cytosine (C). The order of these bases determines genetic codes of the organisms and the biological information has been passed down from generation to generation through the replication of DNA. For this reason, to date, decoding DNA and its biomedical and biochemical applications have received a considerable amount of attention in the last decades and global research activities have been inspired by industry and government agencies.[1,2] More recently, the application of DNA has been extended to the electronics due to its intrinsic benefits such as its natural plenitude, bio-degradability, bio-functionality and low-cost.[3–7] For example, DNA polymer was applied as an electron blocking layer for enhancing the light emission efficiency of organic light-emitting diodes (OLEDs),[8] and also used as a dielectric layer for organic field-effect transistors (OFETs).[9] In addition, the DNA-base small molecule, guanine has been successfully demonstrated as a hydrogen getter for stable operation of FETs and a charge trapping layer for logic applications.[10,11] These previous electric/optoelectric applications have pointed out that DNA host and base are useful but only as passive components rather than active ones; the electrical property of DNA is quite insulating and the thickness of DNA in the previous reports was relatively thick (> 10 nm). Here, we thus recognize that if DNA layer can be scaled down below 10 nm sustaining its insulating properties, it could be useful allowing carrier transport through the thickness by quantum tunneling. Hence, a few nm thickness of DNA may show its functionality as an active layer in

tunneling devices. However, still challenging is whether such an ultra-thin soft organic layer could sustain its insulating properties without current leakage between two electrodes. As revealed in previous reports, conventional vapor-deposited metals such as Au, Al and Ti easily migrate into the ultra-thin soft layer and create the electrical shorts.[12–14] Many researchers have made a great deal of effort to resolve the metal penetration issue suggesting several techniques: low temperature vapor deposition to minimize the metal atom diffusion into organic tunneling layer,[12] using a conducting organic material (PEDOT:PSS) as a buffered electrode,[13] and introducing a liquid metal such as Hg[15,16] or an eutectic alloy of gallium and indium.[17] Although these approaches were conducted for promising results, device yield appeared disappointingly low in fact, and of course DNA layer has never been attempted. Here we report the metal-insulator-metal tunnel diode, which includes 1.35 nm thin two dimensional (2D) synthetic DNA between Au and conducting NiO_x for bottom and top electrodes respectively. The ultra-thin 2D DNA nanosheet was synthesized by simple drop casting of DNA solution and subsequent self-aligning of DNA molecules. Semi-transparent conducting oxide, NiO_x was directly deposited on the DNA layer by thermal evaporation. Our tunneling devices were reproducibly fabricated with high yield over 75%. We regard that our results using the DNA molecules would be world first for active electron device layer applications, and thus believe that our results would inspire any further study toward nanoelectronics using biomolecules.

The DNA molecular device was fabricated in the basis of two-dimensional (2D) double-crossover (DX) DNA lattices.[18–21] The double crossover (DX) DNA lattices are two-dimensional periodic lattices self-assembled with thousands of two repeating DX tiles, where two DNA double-helices with two crossover points as shown in **Figure 1a and b**. Each tile has 4 individual strands and a dimension of each tile is a width of 4 nm and length of 12 nm. According to Figure 1a, a unit DX tile was organized into two crossover junctions where two

parallel duplexes were tied up. We conducted the atomic force microscopy (AFM) measurement in order to verify the DX DNA lattice formation and a representative AFM image with a section profile was displayed in Figure 1b. Although a single DNA duplex had a 2 nm diameter,[22] average height of the DX DNA lattices bound on the substrate in liquid was 1.35 ± 0.2 nm due to the electrostatic attraction between negatively charged DNA and a substrate as depicted in the inset of the Figure 2b. The noise-filtered 2D spectrum image reconstructed by the fast Fourier transforms showed the periodicities of the unit DX tiles along the DNA duplex direction and the perpendicular to the duplex. The ultraviolet-visible (UV-Vis) spectrophotometry of the DNA nanosheets on mica substrate was also performed at an ambient condition to obtain the highest occupied molecular orbital (HOMO)-lowest unoccupied molecular orbital (LUMO) and optical band gap of DX DNA lattices as well from the absorption spectrum. **Figure 1c** and the inset showed the variation in the absorption coefficient (α) as a function of the photon energy (E) and the absorbance spectrum (typical DNA absorption occurred at 260 nm) as a function of the wavelength of the DX DNA lattices, respectively. The fundamental absorption bands associated with the optical band gap (represented as the $\pi \rightarrow \pi^*$ electronic transition) indicate a superposition of the corresponding HOMO-LUMO transitions in DNA molecules. Another strong absorption band placed next to the fundamental absorption band located at the high-energy tail came from the superposition of the second absorption bands of DNA.[23,24] The DX DNA lattices exhibited a clear optical band gap of 4.72 eV and second band onset of 5.30 eV shown in Figure 1c. Our measurement of the optical band gaps revealed slight discrepancies (~ 5%) compared to the previous reports, [25–27] due to the differences in the geometry, number of nucleotides, and interfacial characteristics.

For device fabrication, a 50 nm-thick Au bottom electrode was initially deposited by DC sputtering and patterned on the cleaned Si/SiO_2 substrate. Then, 100 μL of the DX DNA sample solution was drop-casted on the top of the electrode, followed by air-drying for a few

hours and gentle washing with deionized water. This process was repeated several times, eventually to achieve an ultra-thin insulating layer. The self-assembly process of the DNA molecules takes place within the DNA molecules (Guanine with Cytosine and Thiamine with Adenine), whereas commonly used self-assembled monolayers (SAMs) react with the substrate: thiols SAMs works on the surface of Au and phosphonic acid SAMs are only attached on the hydroxyl terminated surface such as AlO_x. We believe that this process for 2D nanosheet DNA layer is one of the most important advantages of our present work. As in the cross-sectional transmission electron microscopy (TEM) images in **Figure 2a**, the interface between DNA and a top electrode of NiO_x was clearly identified due to high electron density of the NiO_x and the thickness of DNA layer was about 1.5 nm, which coincides with the previous results of the atomic force microscopy. This ultra-thin and insulating DNA nanosheet could offer the functionality of the device through the quantum tunneling if top electrode deposition is successful. But the deposition of top electrode on the soft layer appeared still very challenging because of aforementioned metal penetration issue on the ultra-thin soft layer. To this end, the semi-transparent conducting oxide NiO_x was conceived as an excellent option for a top electrode of the DNA based device. The NiO_x has been frequently used for the source and drain electrodes of p-channel organic transistors due to its deep work function of ~5.1 eV. [28,29] Indeed, as thermally evaporated, the interfacial nature between NiO_x and its contacting semiconductors often appeared to be van der Waals interaction rather than chemically-bounded interaction.[30] We thus selected Ni-rich NiO_x (~50 nm, x= ~0.9) as a promising candidate for the top electrode material for molecular devices, expecting its van der Waals-like interaction without any Ni metal diffusion to our ultra-thin DNA layer. It is probably because Ni and O make their compound state on DNA surface without any surface diffusion/contamination.

Figure 2c showed the current-voltage (I-V) characteristics of our DNA tunneling diode with a top NiO_x and bottom Au electrode (NiO_x/DNA/Au), which is compared to those of the

other DNA diode with two Au electrodes (Au/DNA/Au). While the Au/DNA/Au diode and Au/NiO_x without the DNA layer directly showed electrical short, our diode of NiO_x/DNA/Au displayed rectification behaviour; the current density was below 10^{-4} A/cm^2 in a low bias regime less than $\pm$0.3 V, but when the bias does above $\sim$0.3 V the density across the junctions increases exponentially reaching to ~6×10^{-3} A/cm^2 at the bias of 1 V. Moreover, the device yield was over 75 % which is incomparably higher than that from other approaches in molecular electronics,[12,31] as shown in the semi-log plot of the counts versus the current densities (**Figure 2d**, where the plot was prepared by taking log scale on the current density $\times$ 10^4). The number of "working" devices (no electrical short) was 33 among total 43 fabricated and all the current-voltage characteristics of our total number of devices were presented in the supplementary section 1. In order to confirm the effects of NiO_x on the soft layer, the same conducting oxide was applied as the top electrode for a metal-insulator-metal tunneling diode based on self-assembled monolayers (SAMs) and the operation of diode was verified (See supplementary section 2). Therefore, the Ni-rich NiO_x layer is regarded as an excellent electrode material for good contact with general molecular/organic layers.

Our DNA-based diode must not be a resonant tunneling diode but its characteristics were so reversible and reproducible under applied bias sweep, showing tunneling properties. Main transport mechanism of the device might thus be Fowler-Nordheim Tunneling. In order to make sure of the carrier transport mechanism, a temperature-variable current-voltage measurement was attempted and carried out at temperatures from 90 K to 300 K in an increment of 30 K as shown in **Figure 3a**. In our metal-insulator-metal devices, the carrier can be transported through a ultra-thin (< 10 nm) triangular barrier at high applied bias, based on Fowler-Nordheim Tunneling, for which the current density is expressed as in the Equation 1.[32,33]

$$J = \frac{q^2E^2}{8\pi h\phi_B} exp(-\frac{8\pi\sqrt{2m^*(q\phi_B)^3}}{3qhE} \quad (1)$$

where J is the current density, m^* is the effective electron mass in the dielectric layer, q is the electronic charge, $q\phi_B$ is the Schottky barrier height, E is the electric field.

According to Figure 3a, the current density measurement characteristic on our DNA device exhibits temperature-independent characteristics in a temperature range from 120 K to 90 K although the current density gradually changes to decrease with the temperature decrease in the other range from 300 K to 150 K (the inset Figure. 3a also shows the temperature-dependent current characteristics at three different applied voltages of 0.1, 0.5, and 1 V). It is thus highly regarded that the Fowler-Nordheim Tunneling indeed took place in our DNA devices. Additionally, the Fowler-Nordheim (FN) Tunneling Equation 1 can be modified as Equation 2, which clearly express the relationship between ln (J_{FN}/E^2) and $1/E$ to be linear and plotted with a negative slope. The slope represents the Schottky barrier height between the metal and the insulator.

$$\ln\left(\frac{J}{E^2}\right) = \ln\left(\frac{q^2}{8\pi h\phi_B}\right) - \frac{8\pi\sqrt{2m^*}}{3qh}\frac{(q\phi_B)^{3/2}}{E} \quad (2)$$

As shown in **Figure 3b and c,** negative slopes of the curves at a turning voltage (V_T) of $\pm$ 0.3 V are clearly observed at all measurement temperatures. Therefore, we concluded that Fowler-Nordheim (FN) tunneling is the dominant charge transport route in the junctions since negative slopes of the curves at a turning voltage are clearly observed at all measurement temperatures[34] although thermionic Schottky and Poole-Frenkel emissions are partially involved in the conduction through the DNA nanosheets in the high-temperature regime (> 150 K). In fact, at the low temperatures below 120 K, tunneling was only observed. (For details, the charge transport of our DNA devices was analyzed according to four possible conduction mechanisms: direct tunneling, Fowler-Nordheim tunneling, Schottky emission, and Poole-Frenkel emission. See supplementary section 3.) Now, assuming the effective mass

of electrons in DNA as $0.5m_e$, the Schottky barrier heights of Au/DNA and NiO_x /DNA junctions are estimated to be 0.56 and 0.52 eV respectively from the slopes of Fowler–Nordheim plots at the temperature of 90 K in Figure 3c (which were extracted from positive and negative voltage sweep curves in Figure 3b above the turning voltage). Those apparent Schottky barrier heights are plotted as a function of temperature in **Figure 3d,** where barrier height slightly becomes smaller at a higher temperature in measurement and it increases with lighter m_e. However, we can recognize that the genuine Schottky barrier must be the value at the low temperatures, because at 90 and 120 K the barrier height for FN tunneling appears the same although such barrier lowering slightly appears over 150 K. Assuming these genuine barrier heights (0.56 and 0.52 eV) and using the band diagrams of Au/DNA layer/NiO_x system (**Figure 4a**), we could deduce the work function values of Au and NiO_x, to be 5.10 and 5.06 eV. The values could be obtained because we already have the information on the band gap, HOMO, and LUMO levels of our DNA layer as discussed in Figure 1, and those work functions are in well accordance with reported values.[35,36] For the band diagram, exciton binding energy in DNA was not considered but hopefully small enough to be ignored. Now, we regard that the carrier transport is initially blocked by the Schottky barrier between the electrode and the DNA layer in the low bias regime till the turning voltage of 0.3 V. But when the bias exceeds the voltage, Fowler–Nordheim triangular potential gradient forms to allow massive carriers transport though tunneling as interpreted in **Figure 4b and c.**

As our final work to confirm the tunneling properties of the DNA device and to explore any potential applications as well, we attempted electrodynamic response measurements of a DNA tunnel diode. For the measurement, a simple first-order high-pass filter configuration was used as shown in the circuit of **Figure 5a**, where the DNA tunnel diode was connected to a load resistor of 10 MΩ in series and the output voltage (V_{out}) signals were measured as square wave input voltage (V_{in}) signals were entered at a frequency of 0.5 Hz. In a conventional high-pass filter, any low frequency input voltage is always blocked by the filter

capacitor, resulting in no output voltage. On the other hand, the DNA tunnel diode as a filter blocks only low voltage input at a low frequency, passing high voltage input to generate current. **Figure 5b** showed these dynamic responses of a DNA tunnel diode. At the input voltage of 0.2 V below V_T, the voltage transfer characteristics were hardly detected but RC-induced boost-up peaks, which indicate that our DNA layer is an insulating capacitor.[37] At the input voltage of 1 V, the voltage transfer characteristics were clear enough to gain V_{out} and generate current. The sufficient input voltage enables the carriers to tunnel through the DNA layer, now changing the characters of DNA layer as a resistor (see the voltage ranges as insulator and resistor/conductor in Figure 2c). As a result, output voltages are dynamically gained in a reversible form. We regard that our DNA tunnel diode is very similar to Zener diode in functionality and its reversible dynamic response would be very useful for reliable electronics with biomolecules.

In summary, we have fabricated a metal-insulator-metal tunnel diode, which has 1.35 nm ultra-thin 2D synthetic DNA between Au and conducting Ni-rich NiO_x electrodes. The ultra-thin 2D DNA nanosheet was synthesized by simple drop casting of DNA solution and subsequent self-aligning of DNA molecules. Semi-transparent conducting oxide, NiO_x was directly deposited on the DNA layer by thermal evaporation, expected to make van der Waals interface with DNA layer. Our tunneling devices demonstrate reproducible performances with high yield over 75%, displaying FN tunneling properties that statically and dynamically start at 0.3 V. Such reproducible properties promise Zener diode-like device applications using DNA. We conclude that our results applying the DNA molecules for active electron devices must be novel enough to inspire any further study toward nanoelectronics using biomolecules.

Experimental Section

Construction of DX DNA lattices: Synthetic oligonucleotides of DNA purified by high performance liquid chromatography are purchased from Bioneer (Daejeon, Korea). A 2-dimensional DX DNA lattice consisted of two double-crossover (DX) tiles (each tile has four distinct oligonucleotides) is constructed by a free solution annealing process. DX DNA lattices are formed by mixing a stoichiometric quantity of each strand in 1× TAE/Mg^{2+} buffer (40 mM Tris, 20 mM Acetic acid, 1 mM EDTA (pH 8.0), and 12.5 mM magnesium acetate). A test tube containing DX strands (placed in a Styrofoam box having 2 L of boiled water) are cooled slowly from 95 to 25 ℃ for at least 24 hours to facilitate hybridization. The final concentration of DX DNA lattices is 200 nM.

AFM imaging: 30 μL of 1× TAE/Mg^{2+} buffer is dropped onto a freshly cleaved mica surface followed by the deposition of 5 μL of DX DNA sample solution. AFM images are obtained by a Digital Instruments Nanoscope III (Vecco, California, USA) with a multimode fluid cell head in tapping mode under a buffer using oxide-sharpened silicon nitride AFM tips (NP-S, Vecco, California, USA).

Absorption measurement: A spectrophotometer (Cary 5G, Varian, California, USA) is used to conduct the optical absorbance measurement of the DX DNA lattices in the visible and UV regions (wavelength between 800 and 190 nm). The apparatus is equipped with two light sources [a deuterium arc lamp (for near-infrared and visible) and a quartz W−halogen lamp (UV)] and two detectors [a cooled PbS detector (for near-infrared) and a photomultiplier tube (visible and UV)]. The spectrophotometer measures the frequency-dependent light intensity passing either through a vacuum or through the sample.

Device Fabrication: On a cleaned p-Si/SiO_2 substrate, a 50 nm-thick Au bottom electrode was initially deposited by DC sputtering and patterned on the cleaned Si/SiO_2 substrate. Then, 100 μL of the DX DNA sample solution was drop-casted on the top of the electrode, followed by air-drying for a few hours and gentle washing with deionized water. This process was repeated several times, eventually to achieve an ultra-thin insulating layer. After construction of DX DNA lattices, top NiO_x /Au electrode (50 nm/100 nm) was thermally evaporated through a shadow mask.

Temperature-dependent current-voltage characterization and electrodynamic response measurement: A liquid-nitrogen cooling cryostat was used for temperature-variable current-voltage measurement. The temperature range was from 90 K up to 300 K. Current (or current density)-voltage (I-V, or J-V) data was recorded with a semiconductor parameter analyzer (Agilent Technologies). Dynamic response of the device was observed and obtained with a function generator (AFG 310, Sony/ Tektronix).

Supporting Information

Supporting Information is available from the Wiley Online Library or from the author.

Acknowledgements

M.Y. and S-W.M and contributed equally to this work. The authors acknowledge the financial support from NRF (NRL program: Grant No. 2017R1A2A1A05001278, SRC program: Grant No.2017R1A5A1014862, vdWMRC center).

Received: ((will be filled in by the editorial staff))
Revised: ((will be filled in by the editorial staff))
Published online: ((will be filled in by the editorial staff))

References

[1] J. R. Epstein, J. A. Ferguson, K. H. Lee, D. R. Walt, *J. Am. Chem. Soc.* **2003**, *125*, 13753.

[2] K. L. Gunderson, S. Kruglyak, M. S. Graige, F. Garcia, B. G. Kermani, C. Zhao, D. Che, T. Dickinson, E. Wickham, J. Bierle, D. Doucet, M. Milewski, R. Yang, C. Siegmund, J. Haas, L. Zhou, A. Oliphant, J. B. Fan, S. Barnard, M. S. Chee, *Genome Res.* **2004**, *14*, 870.

[3] H. Yan, S. H. Park, G. Finkelstein, J. H. Reif, T. H. Labean, *Science* **2003**, *301*,1882.

[4] G. Maruccio, P. Visconti, V. Arima, S. D'Amico, A. Biasco, E. D'Amone, R. Cingolani, R. Rinaldi, S. Masiero, T. Giorgi, G. Gottarelli, *Nano Lett.* **2003**, *3*, 479.

[5] N. C. Seeman, *Nature* **2003**, *421*, 427.

[6] E. Braun, Y. Eichen, U. Sivan, G. Ben-Yoseph, *Nature* **1998**, *391*, 775.

[7] K. Keren, R, Berman, E. Buxhtab, U.Sivan, E. Braun, *Science.* **2003**, *302*, 1380 .

[8] A. J. Steckl, *Nat. Photonics* **2007**, *1*, 3.

[9] J. Lee, H. Hwang, S. W. Min, J. M. Shin, J. S. Kim, P. J. Jeon, H. S. Lee, S. Im, *ACS Appl. Mater. Interfaces* **2015**, *7*, 1765.

[10] J. Lee, S.-W. Min, H. S. Lee, Y. Yi, S. Im, *J. Mater. Chem. C* **2014**, *2*, 5411.

[11] J. Lee, J. H. Park, Y. T. Lee, P. J. Jeon, H. S. Lee, S. H. Nam, Y. Yi, Y. Lee, S. Im, *ACS Appl. Mater. Interfaces* **2014**, *6*, 4965.

[12] H. Haick, J. Ghabboun, D. Cahen, *Appl. Phys. Lett.* **2005**, *86*, 84.

[13] H. B. Akkerman, P. W. M. Blom, D. M. de Leeuw, B. de Boer, *Nature* **2006**, *441*, 69.

[14] B. De Boer, M. M. Frank, Y. J. Chabal, Weirong Jiang, E. Garfunkel, Z. Bao, *Langmuir* **2004**, *20*, 1539.

[15] K. Slowinski, M. Majda, *J. Electroanal. Chem.* **2000**, *491*, 139.

[16] K. Slowinski, H. K. Y. Fong, M. Majda, *J. Am. Chem. Soc.* **1999**, *121*, 7257.

[17] R. C. Chiechi, E. A. Weiss, M. D. Dickey, G. M. Whitesides, *Angew. Chemie - Int. Ed.* **2008**, *47*, 142.

[18] T. J. Fu, N. C. Seeman, *Biochemistry* **1993**, *32*, 3211.

[19] E. Winfree, F. Liu, L. A. Wenzler, N. C. Seeman, *Nature* **1998**, *394*, 539.

[20] S. R. Dugasani, J. A. Kim, B. Kim, P. Joshirao, B. Gnapareddy, C. Vyas, T. Kim, S. H. Park, V. Manchanda, *ACS Appl. Mater. Interfaces* **2014**, *6*, 2974.

[21] J. Lee, S. Hamada, S. U. Hwang, R. Amin, J. Son, S. R. Dugasani, S. Murata, S. H. Park, *Sci. Rep.* **2013**, *3*, 2115.

[22] S. H. Park, M. W. Prior, T. H. LaBean, G. Finkelstein, *Appl. Phys. Lett.* **2006**, *89*, DOI 10.1063/1.2234282.

[23] S. R. Dugasani, T. Ha, S. J. Kim, B. Gnapareddy, S. Yoo, K. W. Lee, T. S. Jung, H. J. Kim, S. H. Park, J. H. Kim, *J. Phys. Chem. C* **2015**, *119*, 14443.

[24] S. R. Dugasani, T. Ha, B. Gnapareddy, K. Choi, J. Lee, B. Kim, J. H. Kim, S. H. Park, *ACS Appl. Mater. Interfaces* **2014**, *6*, 17599.

[25] Ö. Güllü, M. Çankaya, Ö. Bariş, A. Türüt, *Appl. Phys. Lett.* **2008**, *92*, DOI 10.1063/1.2936086.

[26] R. G. Endres, D. L. Cox, R. R. P. Singh, *Rev. Mod. Phys.* **2004**, 76, 195

[27] S. Sönmezoğlu, Ö. A. Sönmezoğlu, G. Çankaya, A. Yildirim, N. Serin, *J. Appl. Phys.* **2010**, *107*, DOI 10.1063/1.3447985.

[28] J. W. Lee, J. W. Han, S. K. Lee, J. H. Kim, *Mol. Cryst. Liq. Cryst.* **2009**, *1406*, 37.

[29] D.-J. Yun, S.-W. Rhee, *J. Electrochem. Soc.* **2008**, *155*, H899.

[30] H. S. Lee, S. S. Baik, K. Lee, S. Min, P. J. Jeon, J. S. Kim, K. Choi, H. J. Choi, J. H. Kim, S. Im, *ACS Nano* **2015**, *9*, 8312.

[31] T.-W. Kim, G. Wang, H. Lee, T. Lee, *Nanotechnology* **2007**, *18*, 315204.

[32] F.-C. Chiu, *Adv. Mater. Sci. Eng.* **2014**, *2014*, 578168.

[33] W. Wang, T. Lee, M. A. Reed, *Phys. Rev. B* **2003**, *68*, 35416.

[34] J. M. Beebe, B. Kim, J. W. Gadzuk, C. D. Frisbie, J. G. Kushmerick, *Phys. Rev. Lett.* **2006**, *97*, 1.

[35] A. Kahn, *Mater. Horiz.* **2016**, *3*, 7.

[36] S. Battiato, M. M. Giangregorio, M. R. Catalano, R. Lo Nigro, M. Losurdo, G. Malandrino, *RSC Adv.* **2016**, *6*, 30813.

[37] V. Linko, S. T. Paasonen, A. Kuzyk, P. Törmä, J. J. Toppari, *Small* **2009**, *5*, 2382.

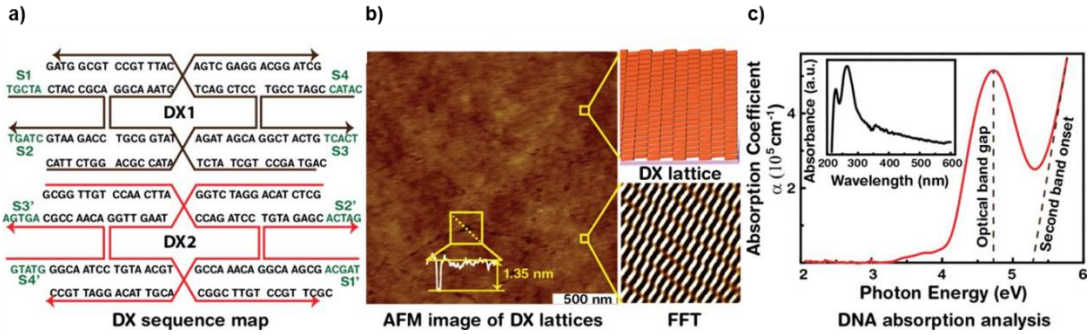

Figure 1. A base-sequence profile of double-crossover (DX) DNA tiles, an AFM image, and absorption of DX DNA lattices. a) DNA sequences of two DX tiles. Each tile consists of four strands, and an arrow in each strand points to the 3' end. The complementary sticky-end pairs are shown as S# and S#' (green). b) A representative AFM image of a DX DNA lattice with a section profile (a scale bar in the image is 500 nm), a schematic of the DX lattice on a given substrate, and the noise-filtered image (scan size of 100 × 100 nm^2) reconstructed *via* fast Fourier transform (FFT) showing clear periodicities of the individual DX tiles. Inset: AFM depth profiles of the DNA nanosheet of 1.35 nm. c) Absorption analysis – absorption coefficient and absorbance spectrum (inset) – of DX DNA lattices on a quartz substrate.

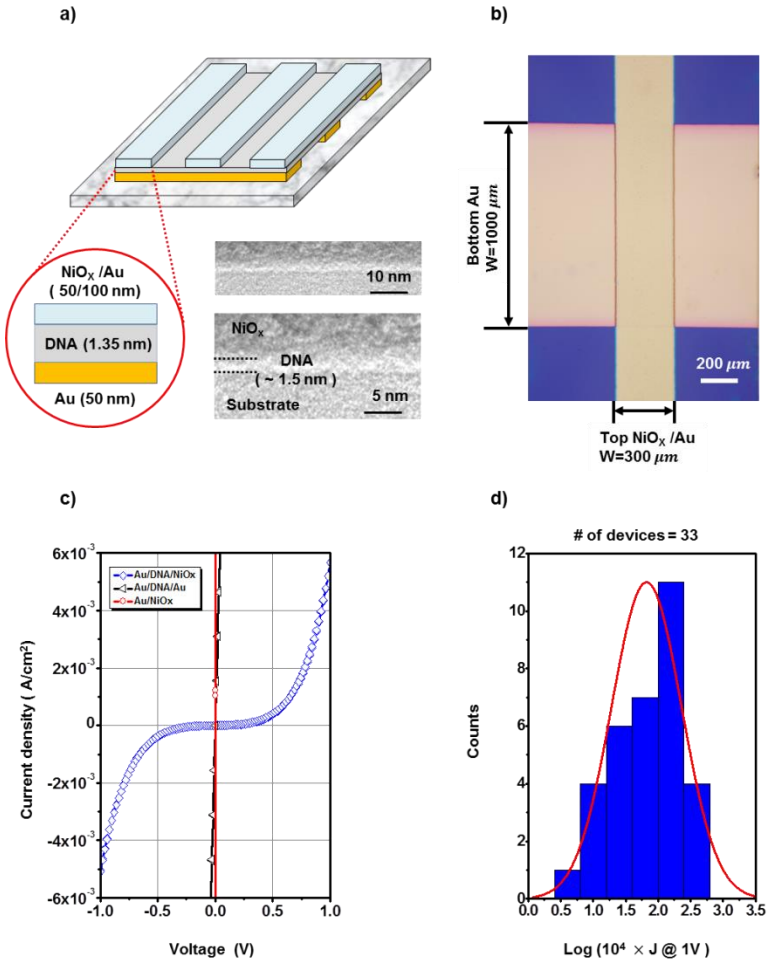

Figure 2. Device structure and characterization. a) Schematic illustration of the crossbar arrays of the metal-insulator-metal tunnel diode with Au/DNA/NiO_x junctions. The ultra-thin DNA nanosheet is sandwiched between a 50 nm-thick Au bottom electrode and a 100 nm-thick NiO_x top electrode. Cross-sectional TEM images of the architecture. The interface between DNA and a top electrode of NiO_x was clearly identified and the thickness of DNA layer was about 1.5 nm. b) Optical microscopic image of the DNA based device (1 cell). The widths (W) of the Au bottom electrode and NiO_x top electrode are 1000 μm and 300 μm, respectively, resulting the cross section area of 3×10^5 μm^2 . c) Current-voltage characteristics of DNA junctions with different top contact materials: NiO_x (blue) presents the FN tunnel diode operation, while Au (black) and NiO_x without the DNA layer (Red) shows electrical shorts. d) Histogram of the logarithmic current densities at 1 V for all "working" DNA based devices. The plot was prepared by taking log scale on the current density (J) × 10^4, and the fluctuation of current is within two orders (J_{min}. 5.4×10^{-4} A/cm^2 at 1 V and J_{max}.4.7×10^{-2} A/cm^2 at 1 V).

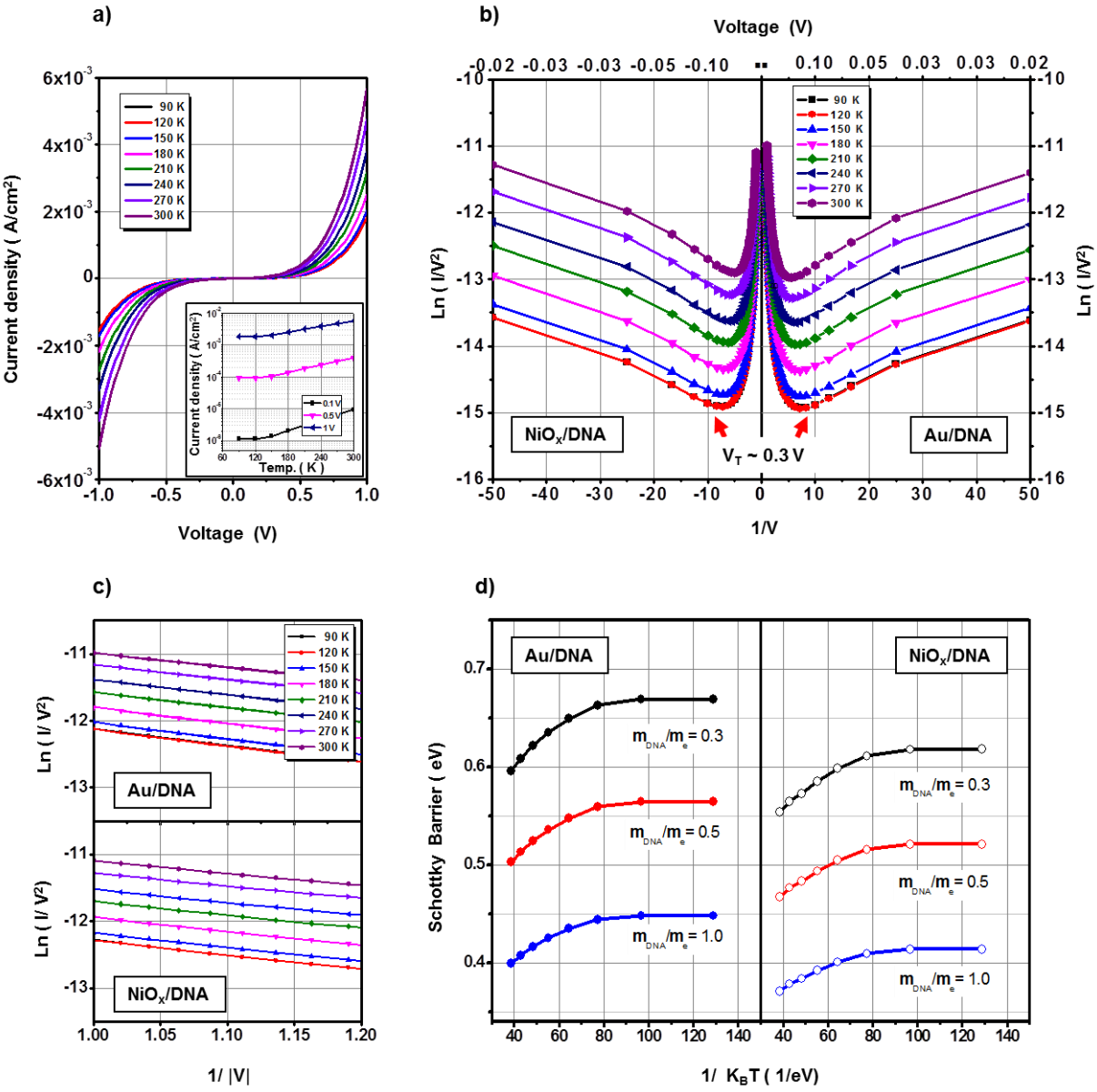

Figure 3. Electric characteristics of the DNA tunneling diode. a) Temperature-variable current-voltage characteristics at temperatures from 90 K to 300 K in an increment of 30 K. The current density of the device gradually decreases as the temperature decreases from 300 K to 150 K. But the current density of the device is maintained as the same value from 120 K to 90. Inset: Current density-temperature plots of the device at the bias conditions of 0.1, 0.5 and 1 V. b) Current-voltage analysis based on Fowler-Nordheim transport model. Negative slope regions above the turning voltage of 0.3 V are displayed in the entire temperature ranges, which indicate Fowler-Nordheim tunneling is the dominant transport mechanism of the junctions. c) FN-plots of Au-DNA junction (as obtained from positive voltage sweep on NiO_x) and FN-plots of NiO_x-DNA junction (negative voltage sweep) for deducing the Schottky barrier heights. d) The estimated apparent Schottky barrier height for the two interfaces. Effective electron mass in DNA is assumed to be 0.3, 0.5, and 1.0 m_e for the calculation. Filled and open circle plots represent the Schottky barrier heights of Au-DNA and NiO_x-DNA, respectively. Genuine Schottky barrier must be the flat value at the low temperatures (<120 K).

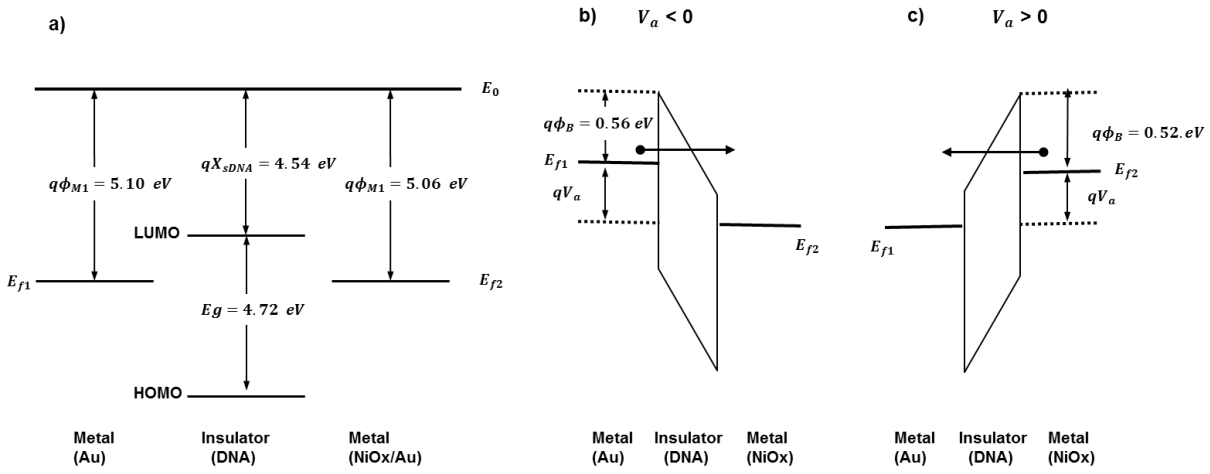

Figure 4. Energy band diagrams of the DNA tunneling diode. a) Energy band diagrams of the Au, DNA and NiO_x, respectively. b,c) Estimated Schottky barrier heights for electron injection from Au and from NiO_x to the DNA layer of 0.56 eV and 0.52 eV, respectively, assuming the effective electron mass of 0.5 m_e .

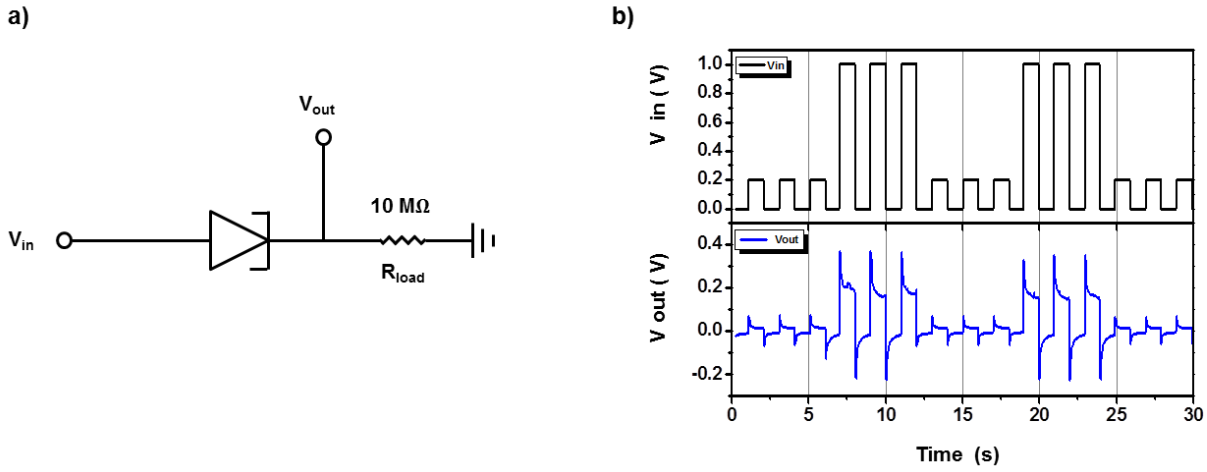

Figure 5. The dynamic responses of a DNA tunnel diode with a load resistor of 10 MΩ. a) A first-order high-pass filter circuit diagram for measurements. b) Voltage transfer characteristics under two square-wave input voltages of 0.2 and 1.0 V at the operating frequency of 0.5 Hz. At the input voltage of 0.2 V below V_T, the voltage transfer characteristics were hardly detected. But at the input voltage of 1 V above V_T, the voltage transfer characteristics are clear enough to gain V_{out} and generate current. The sufficient input voltage enables the carriers to tunnel through the DNA layer, now changing the characters of DNA layer as a resistor.

Table of Contents

The combination of the synthesized two dimensional DNA nanosheets and semitransparent conducting oxide, NiO_x as a top electrode results in the successful operation of non-resonant tunneling diode while temperature-variable current-voltage analysis proves that Fowler–Nordheim tunneling is a dominant conduction mechanism. The DNA-based tunneling appears a promising prototype approach to nanoelectronics using biomolecules.

Keyword: Nanosheet, two-dimensional DNA crystal, semitransparent conducting oxide, tunnel junction diode, charge-transport mechanisms

*Minho Yoon, Sung-Wook Min, Sreekantha Reddy Dugasani, Yong Uk Lee, Min Suk Oh, Thomas D. Anthopoulos, Sung Ha Park and Seongil Im**

***Title** : Charge transport in two-dimensional DNA tunnel junction diodes*

ToC figure

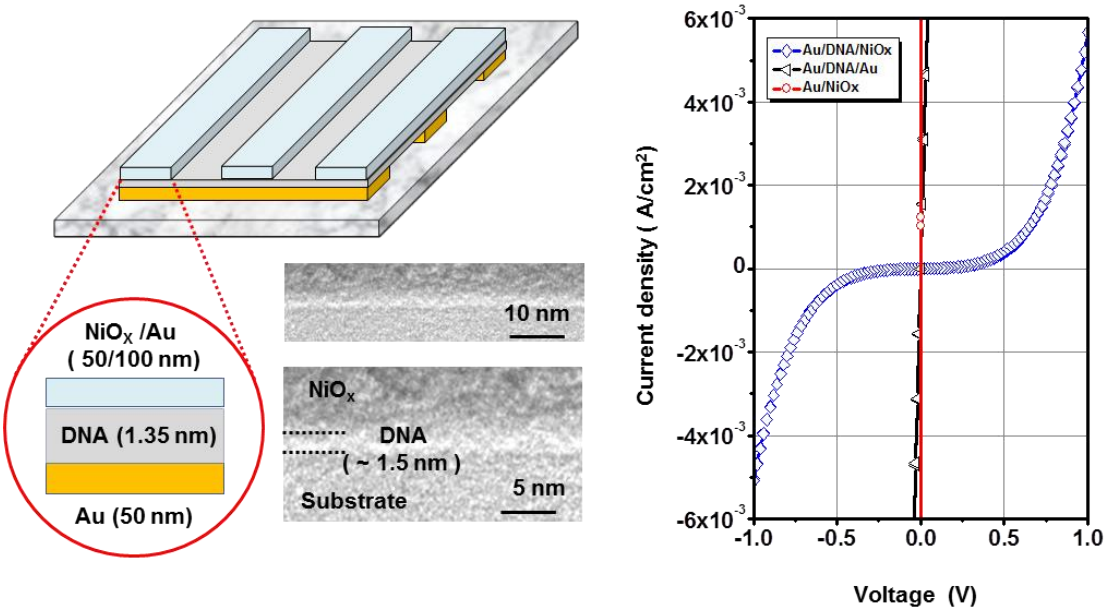

Supporting Information

Title: Charge transport in two-dimensional DNA tunnel junction diodes

*Minho Yoon, Sung-Wook Min, Sreekantha Reddy Dugasani, Yong Uk Lee, Min Suk Oh, Thomas D. Anthopoulos, Sung Ha Park and Seongil Im**

Supplementary section 1: I-V plots showing the uniformity of the DNA tunnel junction diodes. Device yield was 75%.

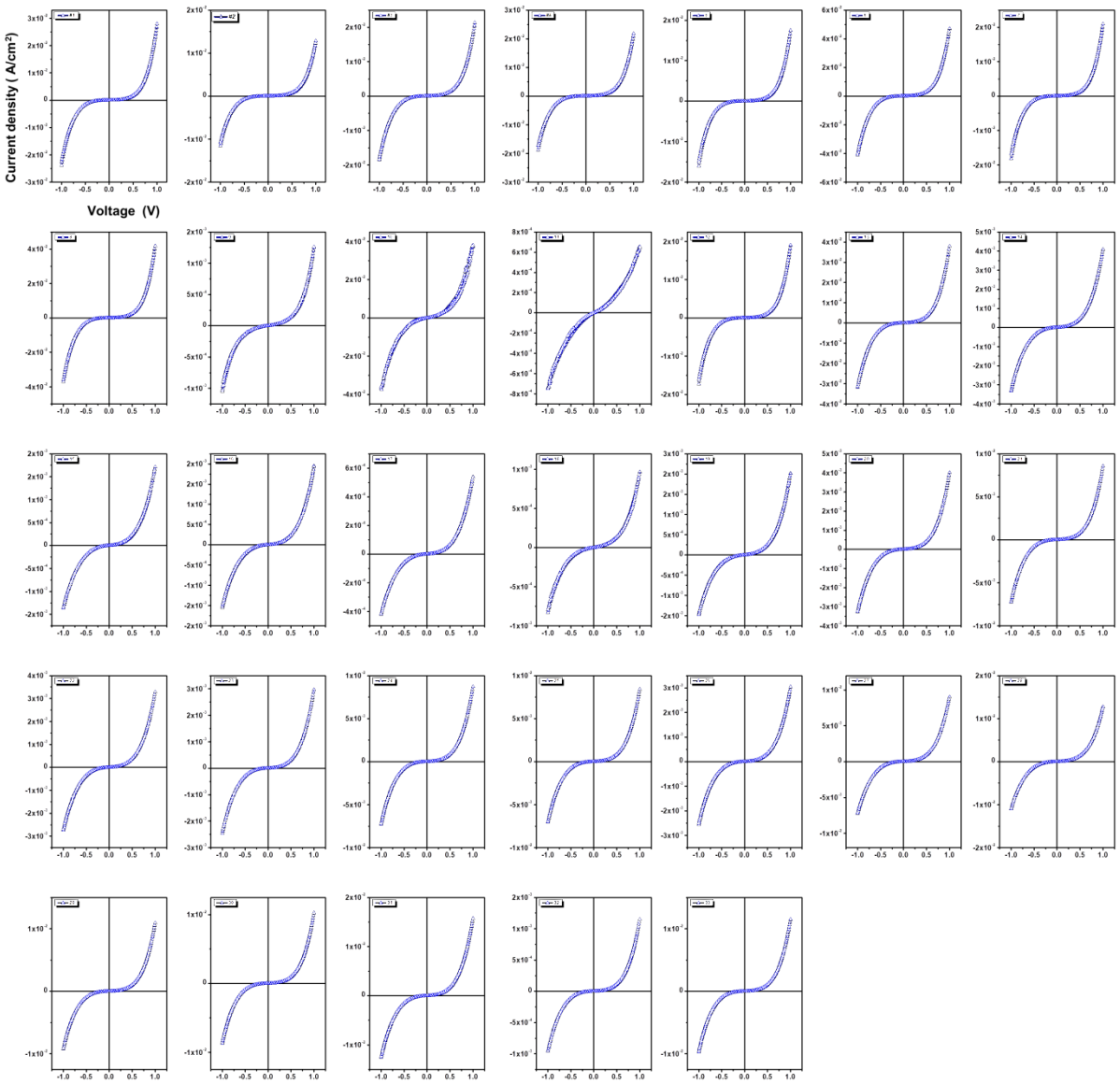

Supplementary section 2

First of all, the optoelectric properties of the NiO_x film were identified. After depositing the semi-transparent 50 nm thick NiO_x films on glass, the resistivity and transmittance of the film were measured. The resistivity using the Van der Pauw method was about 0.1 Ω-cm (Figure S1a), which is more conductive than the conventional semiconducting NiO_x films [1] and comparable to that of the organic conducting material, PEDOT:PSS. [2] This is probably due to the formation of Ni-rich NiO_x rather than the p-type semiconducting and stoichiometric NiO_x film. In addition, transmittance of the film was about 39 % at 550 nm. (Figure S1b) Thus, the semitransparent conducting oxide, NiO_x was would be used for an electrode without any problems.

Next, metal-insulator-metal tunneling diodes based on conventional self-assembled monolayers (SAMs) were fabricated for ensuring the use of the Ni-rich NiO_x layer for overcoming the metal penetration issue on the soft layer. Similarly in the case of DNA based devices, a 50 nm-thick Au bottom electrode was initially deposited by DC sputtering and patterned on the cleaned Si/SiO_2 substrate. The SAM treatment was then performed by immersing the substrates in the SAM solution (2 mM, 1-Octadecanethiol ($C_{18}H_{38}S$) in Ethanol) over 24 hours. [3,4] After rinsing the sample with Ethanol several times and dried with nitrogen gas, the NiO_x was thermally evaporated through a shadow mask, resulting in the cross section area of 3×10^5 μm^2. Figure S2a showed the current-voltage (I-V) characteristics of two SAMs-based diodes with a top NiO_x and bottom Au electrode (NiO_x/SAM/Au), and with two Au electrodes (Au/SAM/Au). Although the current behaviour was asymmetrical, a diode with NiO_x top electrode presented the rectification behaviour, while the Au/SAM/Au diode directly showed electrical short. The current density was below 10^{-6} A/cm^2 in a low bias regime less than ±0.8 V. But when the bias does above ~0.8 V, the current density across the junctions increased exponentially reaching to ~10^{-5} A/cm^2 at the bias of 2 V at 300 K. Moreover, as

shown in the current-voltage analysis based on Fowler-Nordheim transport model (Figure S2b), negative slopes of the curves at a turning voltage (V_T) of 0.8 V was clearly observed as an evidence of FN tunneling. Therefore, to our best knowledge, we confirmed that the Ni-rich NiO_x layer is an excellent electrode material for general molecular/organic layers.

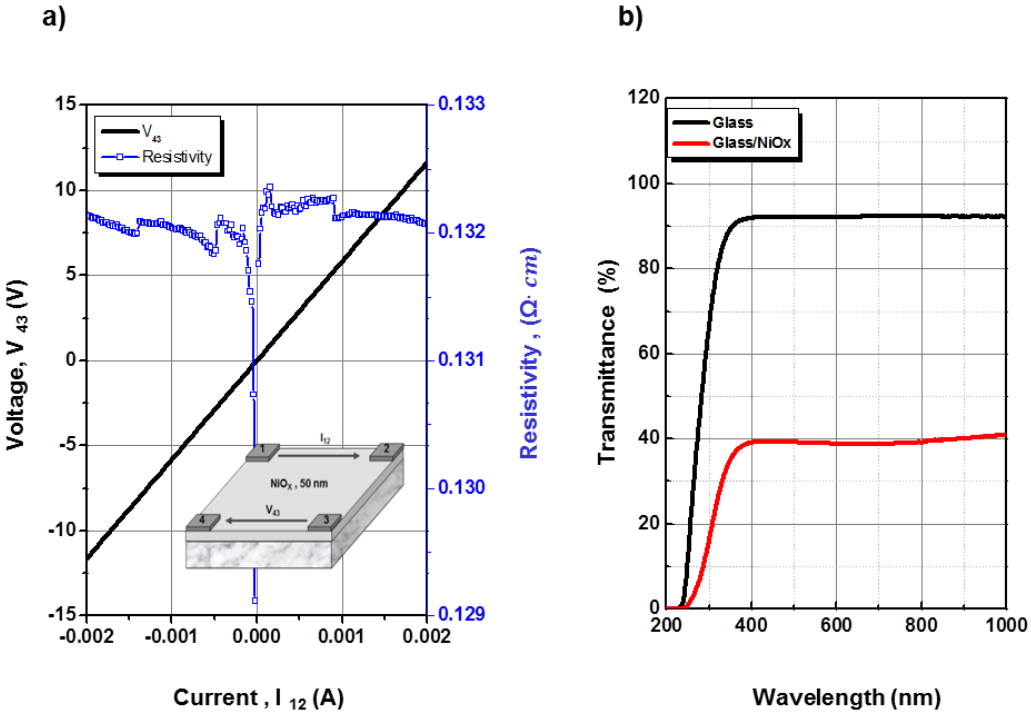

Figure S1. The optoelectric properties of the NiO_x film. a) The resistivity of the Ni-rich NiO_x film. Inset: Schematic illustration of Van der Pauw method for measuring the resistivity. b) Transmittance of NiO_x on glass (red) and glass (black) were 39 % and 92 % at 550nm, respectively.

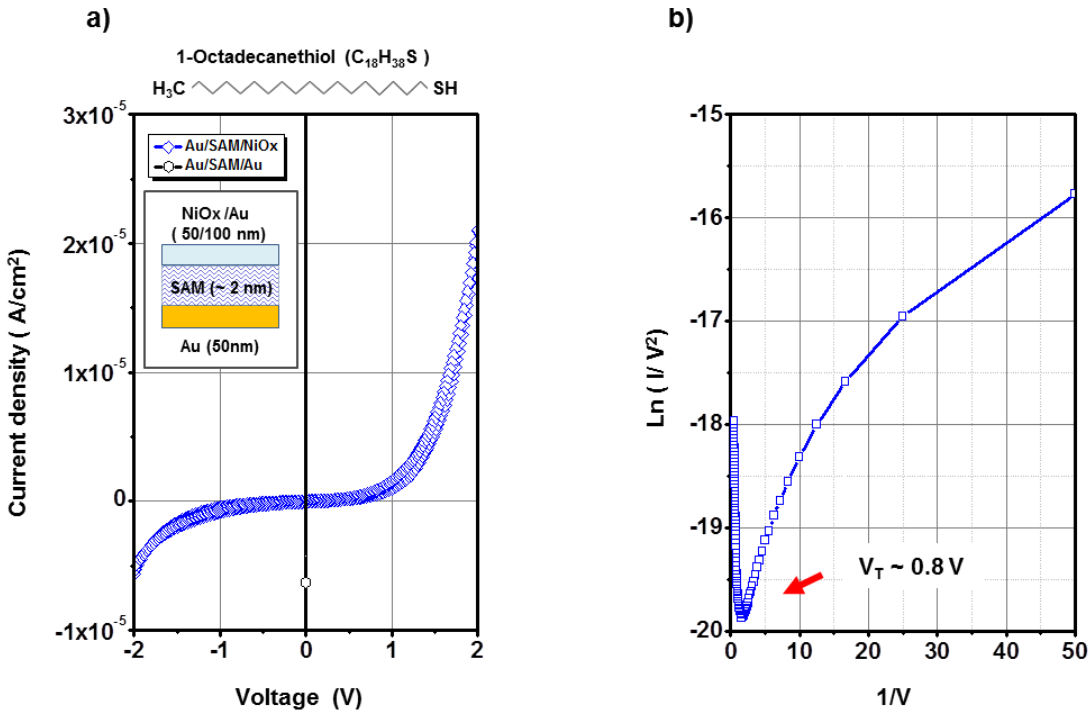

Figure S2. Device structure and characterization. a) Current-voltage characteristics of SAMs, 1-Octadecanethiol ($C_{18}H_{38}S$) based diodes with different top contact materials: NiO_x (blue) presents the diode operation, while Au (black) shows electrical shorts. Inset: Schematic illustration of the device structure of the metal-insulator-metal tunnel diode with NiO_x/SAM/Au junctions. The SAM layer is sandwiched between a 50 nm-thick Au bottom electrode and a 100 nm-thick NiO_x top electrode with the cross section area of 3×10^5 μm^2. **b)** Current-voltage analysis based on Fowler-Nordheim transport model. Negative slope regions above the turning voltage of 0.8 V are displayed at 300 K.

Supplementary section 3

In an effort to investigate the charge transport mechanisms in the Au/DNA/NiO_x junctions, the current-voltage characteristics of as-prepared device were analysed within the framework of the charge transport models: direct tunneling, Fowler-Nordheim tunneling, Schottky emission, and Poole-Frenkel emission.[5–7] Briefly describing with the current-voltage relationships as in the table, if the carrier transport is dominated by direct and Fowler-Nordheim tunneling, the relationships between J and E (direct tunneling) or ln (J/E^2) and $1/E$ (FN tunneling) should be linear with a positive and negative slope respectively. If the current-voltage characteristics were analysed by these two models, the current-voltage relationships appeared to be described by the direct tunneling in the low bias regime (< 0.2 V, see a distinctive linear positive slope for the direct tunneling plot of Figure S3a) and by Fowler-Nordheim tunneling in the high bias regime (> 0.3 V) as shown in the distinctive negative linear characteristics above the turning point of 0.3 V (Figure S3b). However, the current density decreases with the temperature decrease as in the Figure 3a. Hence temperature-dependent transport mechanisms might be partially involved, to be considered for analysing the current transport clearly. If the carrier transport is governed by Schottky and Poole-Frenkel emission, the relationships between ln (J/T^2) vs. $1/T$ and ln (J/E) vs. $1/T$ should be linear, respectively. As shown in the Schottky emission plots of ln (J/T^2) versus $1/T$ (Figure S3c), the curves were rather parabolic with the inflection points near 150 K, indicating that Schottky emission mechanism doesn't work below 150 K. Thus, Schottky emission was regarded to partially involved at the high temperature (> 150 K) low voltage (0.1~0.3 V) regime, but no contribution at the low temperature regime (≤ 120 K). Poole-Frenkel emission seems also involved at such high temperature regime as shown in the Figure S3d, where the relationships between ln (J/E) and $1/T$ keep linear characteristics with negative slopes at high temperatures (>150 K). As the temperature decreases (≤ 120 K), the dependency of ln (J/E) on $1/T$ seems lost indicating no contribution from Poole-Frenkel emission. Therefore, we

conclude that the direct or Fowler-Nordheim tunneling were dominant charge transport routes in the junctions although thermionic Schottky and Poole-Frenkel emissions were partially involved in the conduction at the high-temperature regime (> 150 K).

Conduction Mechanism	*Characteristic Behavior*	*Temperature Dependence*	*Field Dependence*
Direct Tunneling	$J \propto Eexp(-\frac{4\pi d}{h}\sqrt{2m^*\phi B})$	*none*	$J \propto E$
$Fowler-Nordheim$ *Tunneling*	$J = \frac{q^2E^2}{8\pi h\phi_B}exp(-\frac{8\pi\sqrt{2m^*(q\phi B)^3}}{3qhE})$	*none*	$\ln(J/E^2) \propto E^{-1}$
Schottky Emission	$J = \frac{4\pi qm^*k^2T^2}{h^3}exp(-\frac{q\phi_B - \sqrt{q^3E/4\pi\varepsilon}}{kT}$	$\ln(J/T^2) \propto T^{-1}$	$\ln(J) \propto \sqrt{E}$
$Poole-Frenkel$ *Emission*	$J = q\mu N_cEexp(-\frac{q\phi_t - \sqrt{q^3E/\pi\varepsilon}}{kT})$	$\ln(J/E) \propto T^{-1}$	$J \propto E$

Table. Representative charge-transport mechanisms for insulator.

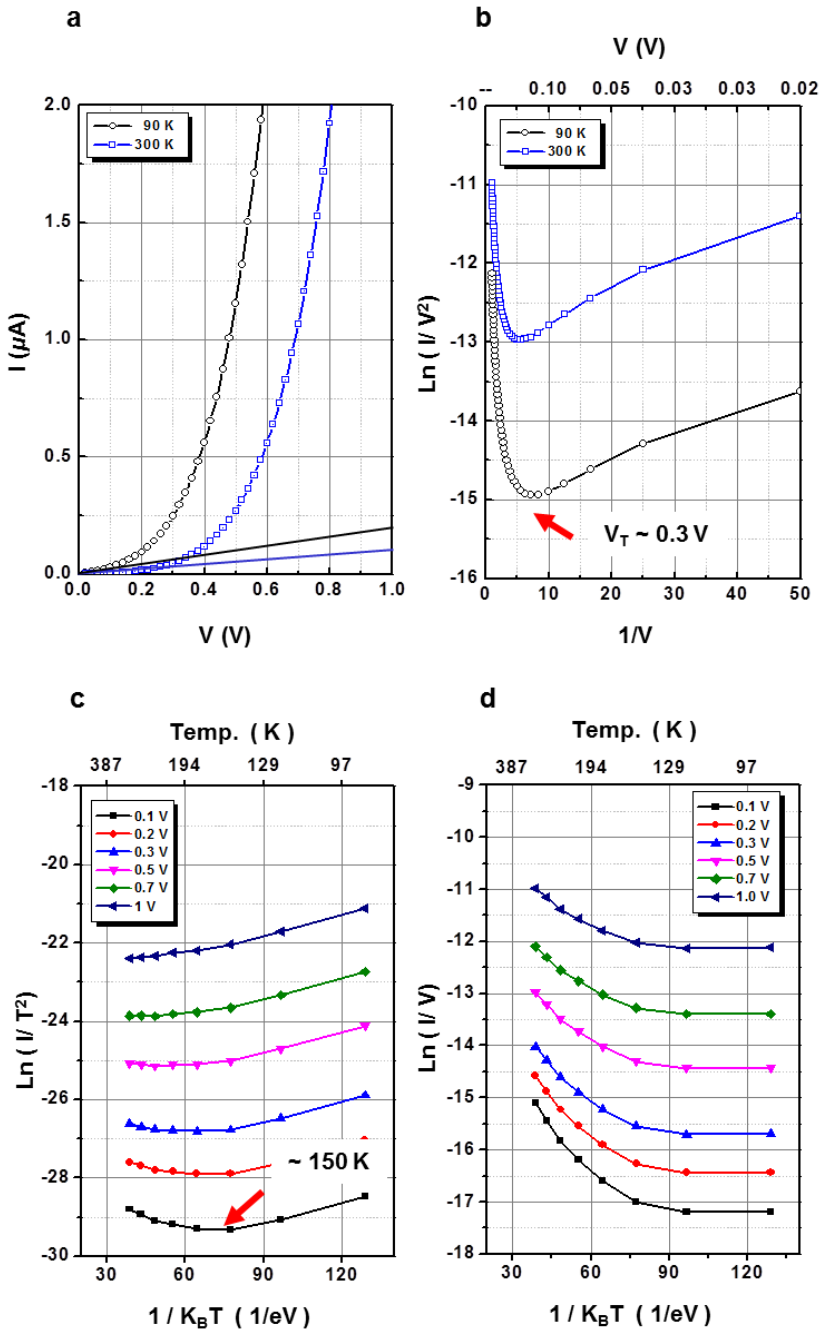

Figure S3. The current-voltage analysis of the DNA molecular device. a) Direct tunneling model at 90 K (black) and 300 K (blue). b) Fowler-Nordheim tunneling model at 90 K (black) and 300 K (blue). The negative slope regions above the turning voltage of 0.3 V are clearly identified. c) Schottky emission model at the bias conditions of 0.1, 0.2, 0.3, 0.5, 0.7 and 1 V. The analyzed curves are parabolic with the inflection points near 150 K. d) Poole-Frenkel emission model at the bias conditions of 0.1, 0.2, 0.3, 0.5, 0.7 and 1 V. At the high-temperature regime (>150 K), the charge transport might partially involve Poole-Frenkel emission. But, As the temperature decreases (≤ 120 K), the linear dependency of ln (*J*/*E*) on 1/*T* was lost, which clearly indicates that Poole-Frenkel emission doesn't work at such low temperature regime.

References

[1] M. Guziewicz, J. Grochowski, M. Borysiewicz, E. Kaminska, J. Z. Domagala, , W. Rzodkiewicz, B. S. Witkowski, K. Golaszewska, R. Kruszkai, M. Ekielski, A. Piotrowska, *Opt. Appl.* **2011**, *XLI*, 431.

[2] B. L. Groenendaal, F. Jonas, D. Freitag, H. Pielartzik, J. R. Reynolds, *Adv. Mater.***2000**, 481.

[3] J. C. Love, L. a. Estroff, J. K. Kriebel, R. G. Nuzzo, G. M. Whitesides, *Chem. Rev.* **2005**, *105*, 1103.

[4] A. Ulman, *Chem. Rev.* **1996**, *96*, 1533.

[5] F.-C. Chiu, *Adv. Mater. Sci. Eng.* **2014**, *2014*, 578168.

[6] W. Wang, T. Lee, M. A. Reed, *Phys. Rev. B* **2003**, *68*, 35416.

[7] J. G. Simmons, *J. Appl. Phys.* **1963**, *34*, 1793.